The Astrophysical Journal, 919:73 (5pp), 2021 October 1 https://doi.org/10.3847/1538-4357/ac1421
© 2021. The American Astronomical Society. All rights reserved.

Anomalous Hα Emission Line Profile Detected at the Center of DDO 53

Justin A. Kader[1], Liese van Zee[1], Kristen B. W. McQuinn[2], and Laura C. Hunter[1]
[1] Department of Astronomy, Indiana University, 727 East 3rd Street, Swain West, Bloomington, IN 47405-7105, USA; jukader@iu.edu
[2] Department of Physics and Astronomy, Rutgers, the State University of New Jersey, 136 Frelinghuysen Road, Piscataway, NJ 08854-8019, USA
Received 2021 February 4; revised 2021 June 10; accepted 2021 July 12; published 2021 September 28

Abstract

We present the detection of a very broad (FWHM $= 670 \pm 17$ km s^{-1}), low-intensity Hα emission line component near the center of DDO 53, a star-forming dwarf irregular galaxy located in the M81 group. The broad component is found at the base of a bright and narrow (FWHM $= 38 \pm 2$ km s^{-1}) component. Using WIYN/Sparsepak optical spectroscopy of the region in addition to multiwavelength archival data, we evaluate the plausibility of several candidate sources, and find that stellar winds from embedded young stars are the most likely origin. However, this result is surprising for such a faint H II region.

Unified Astronomy Thesaurus concepts: Interstellar medium (847); Stellar wind bubbles (1635); Dwarf irregular galaxies (417); Wolf-Rayet stars (1806); Stellar feedback (1602)

1. Introduction

In this paper, we report the detection of an anomalously shaped Hα emission line profile found near the center of DDO 53. As part of a wider project to study the ionized gas kinematics of nearby ($d \lesssim 8$ Mpc) dwarf irregular galaxies, we have fitted and visually inspected over 13,000 fiber spectra falling on classical H II regions, diffuse ionized gas (DIG), OB associations, and supernova remnants (SNRs) in 13 galaxies (J. A. Kader et al. 2021, in preparation). The broad Hα emission line profile reported in this paper is the only one of its kind that we have seen in this large study of ionized gas kinematics.

DDO 53, also known as UGC 04459 or VII Zw 238, is a dwarf irregular galaxy (Hunter & Gallagher 1985; Strobel et al. 1990; de Vaucouleurs et al. 1991; Hunter et al. 1993) located within the M81 group, with a distance modulus of 27.79 (tip of the red giant branch) corresponding to a distance of 3.61 Mpc (Dalcanton et al. 2012). At this distance, the derived H I gas mass is 2.45×10^8 $M_\odot$ (Hunter & Elmegreen 2004), the total stellar mass is 1.91×10^7 $M_\odot$ (Cook et al. 2014), and the current star formation rate is 5×10^{-3} $M_\odot$ yr^{-1} (Hunter & Elmegreen 2004). The distribution of H II regions and the extent of the DIG of this galaxy was studied in detail by Strobel et al. (1990), who described 18 discrete regions. The gas-phase oxygen abundances of three of the brightest H II regions were determined by Croxall et al. (2009), who find the average abundance to be $12 + \log(\mathrm{O/H}) = 7.82 \pm 0.09$.

This paper is organized as follows: in Section 2 we discuss the observations and the reduction of the optical spectra; in Section 3 we explain the analysis techniques and present the results; in Section 4 we enumerate several possible sources of the signal given the observations; and in Section 5 we state our conclusions.

2. Observations and Data

Observations were conducted with the SparsePak multi-object fiber fed spectrograph (Bershady et al. 2004) on the WIYN 3.5 m[3] telescope at Kitt Peak. SparsePak has 82 fibers of diameter 4.″69, adjacent to one another in the core and separated by 11″ in the rest of the field. The 316@63.4 bench spectrograph setup used for these observations includes an X19 blocking filter and an order 8 grating at an angle of 64° for a central wavelength of 6687 Å with a dispersion of 0.306 Å pixel^{-1}. This setup results in a spectral range of 6450–6865 Å, covering the Hα λ6563, [N II] λλ 6548, 6583, He I λ6678, and [S II] λλ 6717,6731 Å emission lines. The bench detector is the STA1 CCD (2600×4000 pix), binned by 4×3 pix, with a gain of 0.438 electrons ADU^{-1}. Bias frames, dark frames, and thorium argon calibration lamp spectra, as well as dome flats and twilight flats were collected each night.

The observations presented here were obtained on UT 2019 December 1 under clear sky conditions. The standard three-point dither pattern that spatially fills the 72″ × 71.″3 field was employed (Bershady et al. 2004). At each of the three dither locations, three 780 s exposures were taken, for a total of nine exposures. Several positions near the center of the pointing will have six or nine independent measurements as a result of the dithering since the core fibers are adjacent to one another and will cover the same positions in multiple pointings. When positions included multiple observations, the final analysis was done using the average of all six or nine individual spectra.

Basic reduction and wavelength solution for the spectroscopic data were performed using the NOAO `HYDRA` package in `IRAF`.[4] Sky continuum and line contributions to the spectra were measured in a dedicated off-galaxy pointing. The sky continuum emission is subtracted from all science spectra. Since sky line emission is variable with time, the individual sky lines were scaled based on their flux in the science frames before subtraction. Residuals from the scaled sky line subtraction were removed by hand using `IRAF/imedit`. Although the science pointing included sky fibers, these were not adequately offset from the galaxy to be used reliably, instead they were used to validate the sky subtraction procedure, i.e., they had nearly zero flux after sky subtraction. The galaxy spectra were smoothed by 1 pixel (0.306 Å) in order to improve the signal-to-noise ratio (S/N). The

[3] The WIYN Observatory is a joint facility of the University of Wisconsin–Madison, Indiana University, the National Optical Astronomy Observatory and the University of Missouri.

[4] IRAF is distributed by the National Optical Astronomy Observatories, which are operated by the Association of Universities for Research in Astronomy, Inc., under cooperative agreement with the National Science Foundation.

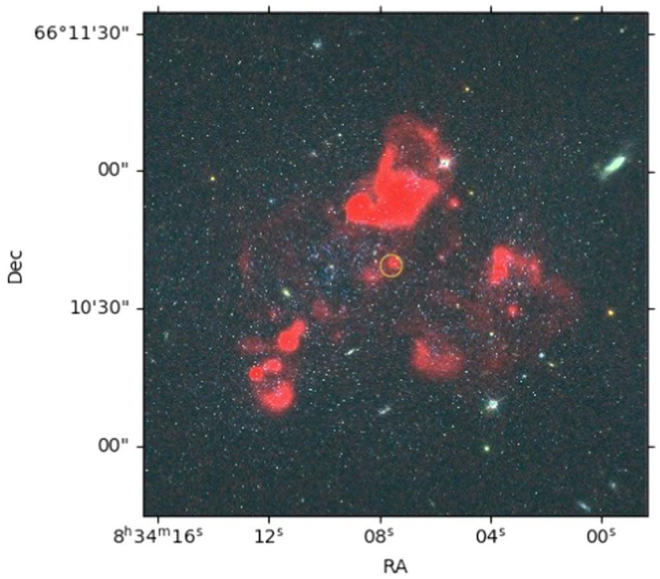

Figure 1. Three-channel image of DDO 53. Blue is the HST ACS/WFC F555W ($\sim V$ band) image, green is the average of the HST ACS/WFC F814W ($\sim I$ band) and the F555W images, and red is the sum of the F814W image and a KPNO 2.1 m narrowband Hα image. The footprint of the SparsePak fiber that included the unusual line profile is shown in yellow.

instrumental contribution to the emission line widths was measured by fitting a Gaussian to several high S/N lines in wavelength calibrated and similarly smoothed thorium argon lamp exposures. The instrumental width (FWHM) for the Hα line in the smoothed spectra was found to be 47.8 ± 1.6 km s^{-1}.

3. Analysis and Results

The SparsePak observations resulted in 246 independent optical spectra across the face of DDO 53. Gaussians were fit to all detected emission lines using the `IDL` software suite `Peak ANalysis` (PAN; Dimeo 2005). Each fiber spectrum was visually inspected in order to determine the number of Gaussian components that would best fit the emission line profiles. In the case of fiber #31, which is shown as a yellow open circle in Figure 1 (R.A. $= 8^{\rm h}34^{\rm m}7\overset{\rm s}{.}6$, decl. $= +66^{\rm d}10^{\rm m}39\overset{\rm s}{.}3$, located on region #11 from Strobel et al. 1990; position S11 hereafter), the Hα emission line profile had an anomalous shape. As illustrated in Figure 2, the profile was best fit by three Gaussians henceforth referred to as C1, C2, and C3 in order of decreasing peak flux. The three components had velocities of $v_{1,\rm Helio} = 17.1 \pm 0.7$, $v_{2,\rm Helio} = 87 \pm 2$, and $v_{3,\rm Helio} = 14 \pm 5$ km s^{-1}. The integrated flux of each component was estimated as the area of the Gaussian fits: 25.2 ± 0.60, 8.94 ± 0.85, and $25.8 \pm 0.47 \times 10^{-16}$ erg s^{-1} cm^{-2} for C1, C2, and C3, respectively. The FWHM values for C1, C2, and C3 were 38 ± 2, 131 ± 5, and 670 ± 17 km s^{-1}, after correcting for the instrumental contribution. For convenience, these Gaussian component parameters are also summarized in Table 1. The Hα emission line profile in the adjacent fiber (#25), at position R.A. $= 8^{\rm h}34^{\rm m}8\overset{\rm s}{.}4$, decl. $= +66^{\rm d}10^{\rm m}36\overset{\rm s}{.}6$, is typical of the rest of the galaxy's nebulae: it is bright and narrow and best fit with a single Gaussian that has FWHM $= 50 \pm 2$ km s^{-1}.

Complex line profiles are usually associated with regions of recent star formation or stellar winds (e.g., Gallagher & Hunter 1984; Skillman & Balick 1984; Martin 1998; Melnick et al. 1999; Points et al. 2019). Usually, these complex kinematics are composed of multiple narrow components. However, the Hα emission line profile at position S11 in DDO 53 displays a shape that is distinct. As is often seen in spectra of regions of recent star formation (J. A. Kader et al. 2021, in preparation), the Hα profile features two fairly narrow blended components; however, this double-component feature (with centroids separated by 69 ± 2 km s^{-1}) is superimposed on a very broad, low-intensity pedestal. This broad component is not significantly separated from the primary component in velocity, but it has a very large velocity width with an FWHM $= 670 \pm 17$ km s^{-1}, significantly in excess of the typical Hα line FWHM (59 ± 27 km s^{-1} among $\sim$13,000 fiber spectra of star-forming regions, J. A. Kader et al. 2021, in preparation; 49.9 ± 6.2 km s^{-1}, Moiseev et al. 2015).

Correspondingly large velocity width components in the [S II] lines in this fiber position were not detected (see Figure 3). The RMS noise of the continuum in fiber 31 is 2.8×10^{-17} erg s^{-1} cm^{-2} Å^{-1}, and the peak flux of the broad Hα component is 1.63×10^{-16} erg s^{-1} cm^{-2} Å^{-1}. Assuming the galaxy-average [S II]/Hα narrow component integrated flux ratio (0.08), we would expect an [S II] broad component peak flux of 1.3×10^{-17} erg s^{-1} cm^{-2} Å^{-1}. Therefore the expected peak flux for a broad [S II] component in the photoionized regime would be below the 1σ level in this spectrum. Among the galaxies studied in J. A. Kader et al. (2021, in preparation), the [S II]/Hα ratio was found in several cases to be as high as $\sim$0.3–0.4. These values are typical for shock ionized low-metallicity gas (Fesen et al. 1985; Stasińska 1990). In this regime, we would expect an [S II] broad component peak flux of $\sim 6.52 \times 10^{-17}$ erg s^{-1} cm^{-2} Å^{-1}, which would only be a marginal detection at the $\sim 2\sigma$ level. Thus, we cannot rule out the possibility of a similar broad component in the forbidden lines.

4. Discussion

It is not exactly clear what astrophysical object or process at position S11 is responsible for such a unique Hα line profile shape. Follow-up observations were obtained on UT 2021 May 4 that have similar spectral signatures in the three components, which rules out any short-term variability of the source. Close examination of archival HST images of DDO 53 (HST proposal 10605) indicates numerous point sources in this fiber position. However, the brightest point source, coincident with the peak in the Hα emission, is blended, so its exact properties cannot be established. We discuss the candidate sources below.

Active galactic nucleus. Recent estimates of the AGN occupation fraction for dwarf galaxies ($M_\star \lesssim 3 \times 10^9 M_\odot$) are typically between 0.4%–1% (Sartori et al. 2015; Pardo et al. 2016; Mezcua et al. 2018), with some authors claiming fractions as high as 30% (Kaviraj et al. 2019; Manzano-King et al. 2019), meaning a significant minority of dwarf galaxies may host AGN. We considered the possibility that this centrally located source is an AGN since Hα emission line profiles of broad-line AGNs can include bright narrow components superimposed on fainter, high velocity width (FWHM $\sim$ 600–1000 km s^{-1}) components (Reines et al. 2013; Baldassare et al. 2016; Manzano-King et al. 2019), and the spectra of AGN in low-metallicity dwarf galaxies do not feature similarly broad components in the low ionization potential [N II]λ6584 and [S II]$\lambda\lambda$ 6713,6731 Å lines (Reines et al. 2013; Sartori et al. 2015; Baldassare et al. 2016). Additionally, Marleau et al. (2017) flag DDO 53 as a candidate

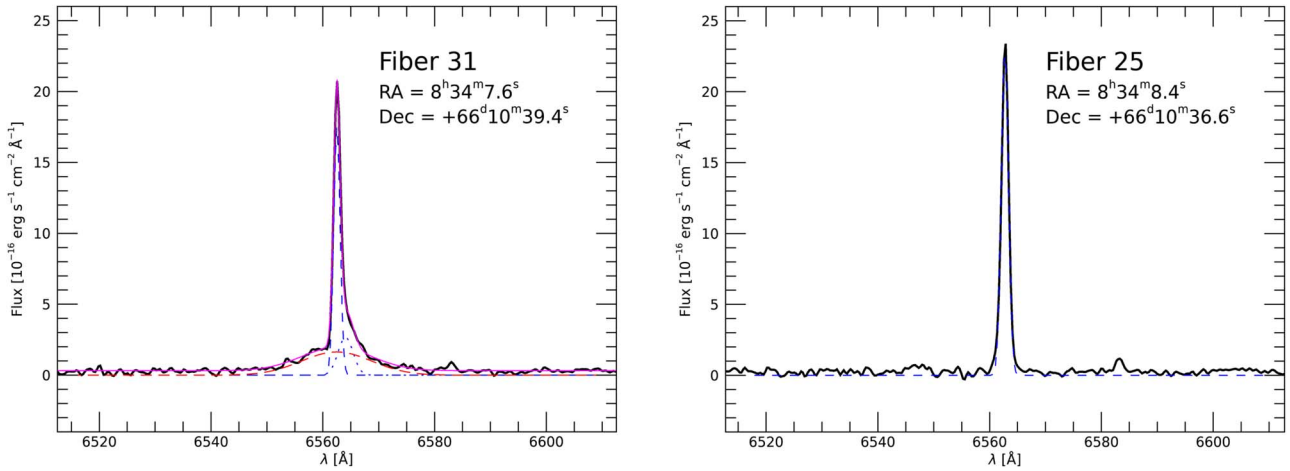

Figure 2. The Hα emission line profile of Fiber 31 (left panel) is fit with three Gaussian components. The primary component, C1 (dashed blue curve), is bright and narrow (FWHM $= 38 \pm 2$ km s^{-1}). The secondary component, C2 (blue dotted curve), is fairly narrow (FWHM $= 131 \pm 5$ km s^{-1}) and is offset from C1 by 69 ± 2 km s^{-1}. The very broad component, C3 (red dashed curve), has FWHM $= 670 \pm 17$ km s^{-1}, and has peak velocity approximately equal to C1. The heliocentric radial velocities of the centroid of each component are $v_{\rm helio} = 17.1 \pm 0.7$, 87 ± 2, and 14 ± 5 km s^{-1} for C1, C2, and C3, respectively. The right panel shows the Hα emission line from the neighboring Fiber #25, which has an FWHM $= 50 \pm 2$ km s^{-1} and a shape that is typical for the rest of the galaxy. The galaxy continuum has been subtracted from both spectra.

Table 1
Fit Parameters to the Hα Emission Line Profile Detected in Fiber 31

	C1	C2	C3
Peak Flux [10^{-16} erg s^{-1} cm^{-2} Å^{-1}]	17.5 ± 0.20	2.66 ± 0.13	1.63 ± 0.02
Integrated Flux [10^{-16} erg s^{-1} cm^{-2}]	25.2 ± 0.60	8.94 ± 0.85	25.8 ± 0.47
FWHM [km s^{-1}]	38 ± 2	131 ± 5	670 ± 17
$v_{\rm Helio}$ [km s^{-1}]	17.1 ± 0.7	87 ± 2	14 ± 5

AGN host galaxy, since their WISE IR photometry indicate a red excess in the W1–W2 color, which is commonly used to select AGN candidates (Stern et al. 2012; Sartori et al. 2015).

However, the WISE source catalog indicates that the red excess reported in Marleau et al. (2017) was measured from the northern main star-forming region and not from S11. The [N II] λ6584/Hα integrated line flux ratio measured in our fiber spectrum is only 0.02, placing the source comfortably in the star-forming region of the BPT diagram (Baldwin et al. 1981; Kewley et al. 2006). We reprocessed archival Very Large Array (VLA) 21 cm data from project codes AH608, AH622, and AW605 to create line maps similar to those in Walter et al. (2008) and continuum maps, and inspected the Chandra events image that includes DDO 53 (Jenkins et al. 2010) and VLA 6 cm continuum maps of DDO 53 (Hindson et al. 2018), but find no evidence of 21 cm or 6 cm continuum (synchrotron radiation) or X-ray emission from S11. For these reasons it is unlikely that the emitter is an AGN.

Supernova remnant. Typical SNRs feature bright Balmer emission as well as emission in the forbidden lines of oxygen, sulfur, and nitrogen originating from shocked ISM that is cooling radiatively. In contrast, the so-called "Balmer-dominated" SNRs exhibit strong Balmer emission with little to no forbidden line emission (Chevalier & Raymond 1978). Spectra from these SNRs have [S II]/Hα ratios well below 0.05 (Lin et al. 2020). The Hα emission line profiles emerging from the nonradiative shocks in the filaments of Balmer-dominated SNRs are characterized by a narrow component superimposed on a broad component with FWHM values ranging from 580 to 2300 km s^{-1} (Smith et al. 1991). We consider the possibility that the source at position S11 is a Balmer-dominated SNR because the observed spectrum is consistent with those characteristics.

While there are similarities between the spectrum from position S11 and that of a Balmer-dominated SNR, i.e., a narrow component superimposed on a lower-intensity broad component, and comparatively weak [N II] and [S II] lines, the absence of any X-ray or nonthermal radio continuum emission from position S11 casts serious doubt on the prospect that the emitter at position S11 is an SNR, since even the Balmer-dominated variety should exhibit thermal X-ray or synchrotron emission.

Wolf–Rayet star. In dwarf irregular galaxies, Wolf–Rayet (WR) stars are found to inhabit giant H II regions and stellar knots (Drissen et al. 1993; Origlia et al. 2001). Several Local Group dwarf irregular galaxies have been surveyed for WR stars: there are 12 known in the SMC, 154 in the LMC, 4 in NGC 6822, and 1 in IC 1613 (Neugent & Massey 2019). We considered whether the source at S11 is a WR star since hydrogen-rich nitrogen sequence (WNh) WR stars contain broadened Balmer emission lines, with FWHM values ranging from $\sim$500 to several thousand km s^{-1}, and lack P Cygni absorption features (Martins et al. 2009; Bestenlehner et al. 2014; Hamann et al. 2019). Although the observed Hα profile is in pure emission, and the broad component has a width compatible with a late-type WNh star, we do not detect the He I λ6678 Å emission line, which is characteristic of massive evolved stars undergoing mass loss and features prominently in the spectra of late-type WNh stars (Drissen & Roy 1994). Therefore it is unlikely that the source of the broad Hα component at S11 is a WR star.

Massive stellar winds. Hα emission line profiles featuring faint, high velocity components have been observed in an increasing number of low-metallicity H II regions (Tenorio-Tagle et al. 1997; Binette et al. 2009). One of the first and most extreme examples was the discovery of a broad (FWHM $=$ 2400 km s^{-1}) Hα emission line component near the center of the supergiant H II region Markarian 71, at the southwest edge of the dwarf irregular galaxy NGC 2366 (Roy et al. 1992;

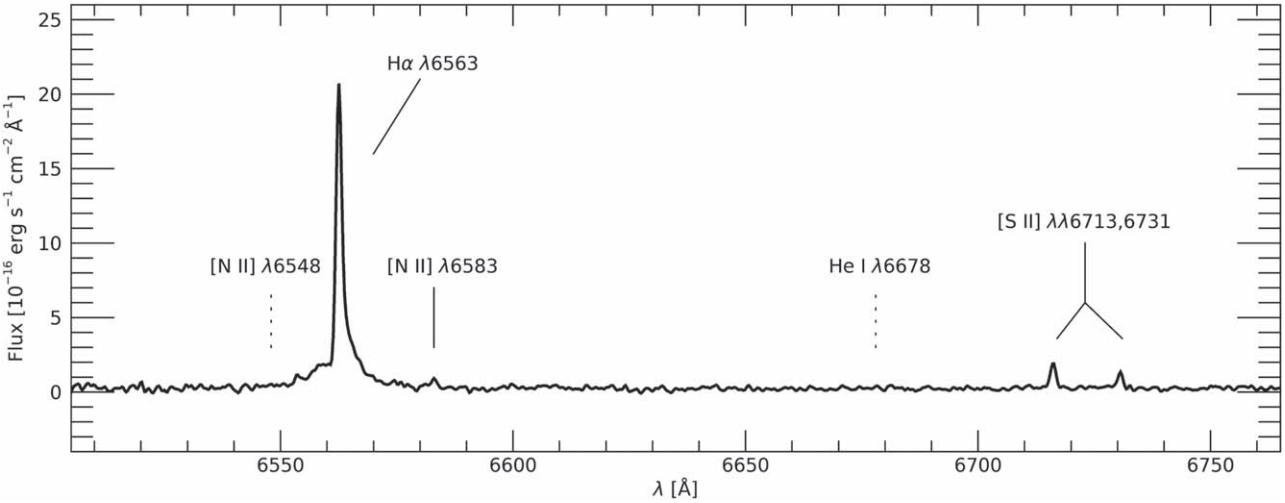

Figure 3. Fiber 31 spectrogram with spectral range cropped to show the detected emission lines. The [N II]λ6584 Å and [S II]$\lambda\lambda$ 6713,6731 Å lines are evident; however, the [N II]λ6548 Å and He I λ6678 Å lines are not detected. We do not detect large velocity width components in the forbidden lines at this fiber position.

Gonzalez-Delgado et al. 1994). Similar broad components in Hα line profiles have been observed in other dwarf irregular galaxies including Haro 3 (FWHM $\sim$2000 km s^{-1}; Tenorio-Tagle et al. 1997), SDSS J143245.98+404300.3 (FWHM $\sim$ 850–1000 km s^{-1}; Del Pino et al. 2019), NGC 4861 (FWHM$_{[O\ III]} \sim$ 1200 km s^{-1}; Izotov et al. 1996), NGC 1569 (FWHM $\sim$ 150 km s^{-1}; Westmoquette et al. 2008), M82 (FWHM $\sim$ 150–350 km s^{-1}; Westmoquette et al. 2009), and the giant H II region NGC 5471 (FWHM $\sim$ 600 km s^{-1}; Castaneda et al. 1990). Typically, these broad components are centered on starburst clumps or bright super star clusters and extend several hundred parsecs across giant or supergiant H II regions, becoming less prominent farther from the center (Westmoquette et al. 2008, 2009). Several hypotheses have been put forward to account for the extended broad component: H II region breakout of fast-expanding shells due to Rayleigh–Taylor instabilities; charge exchange reactions behind the shocks of SNRs; thermal line broadening caused by Thomson scattering in very hot gas; hot stellar winds; and turbulent mixing layers (Roy et al. 1992; Binette et al. 2009; Del Pino et al. 2019). However, there is still no consensus on the origin of extended, faint, high velocity emission line components in H II regions.

Simple scaling relations involving the Hα luminosity of H II regions allow for estimates of the required ionizing radiation and the total mass of ionized gas (Kennicutt et al. 1989; Osterbrock & Ferland 2006). Using a 20 *Å*-wide spectrophotometric filter, the integrated Hα flux inside fiber 31 was found to be $F(\mathrm{H}\alpha) = 5.8 \times 10^{-15}$ erg s^{-1} cm^{-2}, after correcting for interstellar reddening using $E(B-V) = 0.025$ from Youngblood & Hunter (1999) and the algorithm from Cardelli et al. (1989). This flux is consistent with Hα imaging collected during photometric conditions. At an adopted distance of 3.61 Mpc, the corresponding Hα luminosity is $L(\mathrm{H}\alpha) = 9.0 \times 10^{36}$ erg s^{-1}. The required UV input would be 6.6×10^{48} photons s^{-1}, corresponding to either 13 B0.5 V main-sequence stars, two O9 V main-sequence stars, or a single O8 V main-sequence star. Thus, given the brightness of the H II region, it is very surprising that such a high velocity outflow is detected.

5. Conclusions

We have presented observations of an anomalous Hα emission line profile at the center of the gas rich star-forming dwarf irregular galaxy DDO 53. The feature includes two narrow Gaussian components separated in velocity by 69 ± 2 km s^{-1} both superimposed on a very broad low-intensity feature with FWHM $= 670 \pm 17$ km s^{-1}. Based on multiwavelength archival data and follow-up spectroscopic observations, it appears that stellar winds are the most likely source of the anomalous signature. Nevertheless, it is surprising that a very high velocity ionized gas outflow should be associated with such a faint H II region.

The authors thank the anonymous referee for constructive comments. The authors gratefully acknowledge financial support through National Science Foundation grant Nos. 1806926 and 1806522. Any opinions, findings, and conclusions or recommendations expressed in this material are those of the authors and do not necessarily reflect the views of the National Science Foundation. J.A.K. would like to thank the staff at WIYN Observatory for their support during the observing runs. This work was based on WIYN (SparsePak) observations at Kitt Peak National Observatory, the NSF's National Optical-Infrared Astronomy Research Laboratory, which is operated by the Association of Universities for Research in Astronomy (AURA) under a cooperative agreement with the National Science Foundation. This research was based in part on archival VLA observations. The National Radio Astronomy Observatory is a facility of the National Science Foundation operated under cooperative agreement by Associated Universities, Inc. This research has made use of the NASA/IPAC Extragalactic Database (NED), which is operated by the Jet Propulsion Laboratory, California Institute of Technology, under contract with the National Aeronautics and Space Administration. This research has made use of NASA's Astrophysics Data System Bibliographic Services.

ORCID iDs

Justin A. Kader https://orcid.org/0000-0002-6650-3757
Kristen B. W. McQuinn https://orcid.org/0000-0001-5538-2614

References

Baldassare, V. F., Reines, A. E., Gallo, E., et al. 2016, ApJ, 829, 57
Baldwin, J. A., Phillips, M. M., & Terlevich, R. 1981, PASP, 93, 5
Bershady, M. A., Andersen, D. R., Harker, J., Ramsey, L. W., & Verheijen, M. A. 2004, PASP, 116, 565
Bestenlehner, J. M., Gräfener, G., Vink, J. S., et al. 2014, A&A, 570, A38
Binette, L., Drissen, L., Ubeda, L., et al. 2009, A&A, 500, 817
Cardelli, J. A., Clayton, G. C., & Mathis, J. S. 1989, ApJ, 345, 245
Castaneda, H. O., Vilchez, J. M., & Copetti, M. V. F. 1990, ApJ, 365, 164
Chevalier, R. A., & Raymond, J. C. 1978, ApJL, 225, L27
Cook, D. O., Dale, D. A., Johnson, B. D., et al. 2014, MNRAS, 445, 899
Croxall, K. V., van Zee, L., Lee, H., et al. 2009, ApJ, 705, 723
Dalcanton, J. J., Williams, B. F., Melbourne, J. L., et al. 2012, ApJS, 198, 6
de Vaucouleurs, G., de Vaucouleurs, A., Corwin, H. G., et al. 1991, Third Reference Catalogue of Bright Galaxies (New York: Springer), 2091
Del Pino, B. R., Arribas, S., Lopez, J. P., et al. 2019, A&A, 630, A124
Dimeo, R. 2005, PAN User Guide, ftp://ncnr.nist.gov/pub/staff/dimeo/pandoc.pdf
Drissen, L., & Roy, J. 1994, PASP, 106, 974
Drissen, L., Roy, J.-R., & Moffat, A. F. J. 1993, AJ, 106, 1460
Fesen, R. A., Blair, W. P., & Kirshner, R. P. 1985, ApJ, 292, 29
Gallagher, J. S., & Hunter, D. A. 1984, ARA&A, 22, 37
Gonzalez-Delgado, R. M., Perez, E., Tenorio-Tagle, G., et al. 1994, ApJ, 437, 239
Hamann, W.-R., Gräfener, G., Liermann, A., et al. 2019, A&A, 625, A57
Hindson, L., Kitchener, G., Brinks, E., et al. 2018, ApJS, 234, 29
Hunter, D. A., & Elmegreen, B. G. 2004, AJ, 128, 2170
Hunter, D. A., & Gallagher, J. S. 1985, ApJS, 58, 533
Hunter, D. A., Hawley, W. N., & Gallagher, J. S. 1993, AJ, 106, 1797
Izotov, Y. I., Dyak, A. B., Chaffee, F. H., et al. 1996, ApJ, 458, 524
Jenkins, L., Hornschemeier, A., Zezas, A., et al. 2010, AAS HEAD Meeting, 11, 29.05
Kaviraj, S., Martin, G., & Silk, J. 2019, MNRAS, 489, L12
Kennicutt, R. C., Edgar, K. B., & Hodge, P. W. 1989, ApJ, 337, 761
Kewley, L. J., Groves, B., Kauffmann, G., & Heckman, T. 2006, MNRAS, 372, 961
Lin, C. D-J., Chu, Y-H., Ou, P-S., et al. 2020, ApJ, 900, 149
Manzano-King, C. M., Canalizo, G., & Sales, L. V. 2019, ApJ, 884, 54
Marleau, F. R., Clancy, D., Habas, R., et al. 2017, A&A, 602, A28
Martin, C. L. 1998, ApJ, 506, 222
Martins, F., Hillier, D. J., Bouret, J. C., et al. 2009, A&A, 495, 257
Melnick, J., Tenorio-Tagle, G., & Terlevich, R. 1999, MNRAS, 302, 677
Mezcua, M., Civano, F., Fabbiano, G., et al. 2018, MNRAS, 478, 2576
Moiseev, A. V., Tikhonov, A. V., & Klypin, A. 2015, MNRAS, 449, 3568
Neugent, K., & Massey, P. 2019, Galax, 7, 74
Origlia, L., Leitherer, C., Aloisi, A., et al. 2001, AJ, 122, 815
Osterbrock, D. E., & Ferland, G. J (ed.) 2006, Astrophysics of Gaseous Nebulae and Active Galactic Nuclei (2nd ed.; Sausalito, CA: Univ. Science Books)
Pardo, K., Goulding, A. D., Greene, J. E., et al. 2016, ApJ, 831, 203
Points, S. D., Long, K. S., Winkler, P. F., et al. 2019, ApJ, 887, 66
Reines, A. E., Greene, J. E., & Geha, M. 2013, ApJ, 775, 116
Roy, J., Aube, M., McCall, M. L., et al. 1992, ApJ, 386, 498
Sartori, L. F., Schawinski, K., Treister, E., et al. 2015, MNRAS, 454, 3722
Skillman, E. D., & Balick, B. 1984, ApJ, 280, 580
Smith, R. C., Kirshner, R. P., Blair, W. P., et al. 1991, ApJ, 375, 652
Stasińska, G. 1990, A&AS, 83, 501
Stern, D., Assef, R. J., Benford, D. J., et al. 2012, ApJ, 753, 30
Strobel, N. V., Hodge, P., & Kennicutt, R. C. 1990, PASP, 102, 1241
Tenorio-Tagle, G., Munoz-Tunon, C., Perez, E., et al. 1997, ApJL, 490, L179
Walter, F., Brinks, E., de Blok, W. J. G., et al. 2008, AJ, 136, 2563
Westmoquette, M. S., Smith, L. J., & Gallagher, J. S. 2008, MNRAS, 383, 864
Westmoquette, M. S., Smith, L. J., Gallagher, J. S., et al. 2009, ApJ, 696, 192
Youngblood, A. J., & Hunter, D. A. 1999, ApJ, 519, 55